

## University of Dayton eCommons

---

Electrical and Computer Engineering Faculty  
Publications

Department of Electrical and Computer  
Engineering

---

4-2015

# Efficient Thermal Image Segmentation through Integration of Nonlinear Enhancement with Unsupervised Active Contour Model


Fatema Albalooshi  
*University of Dayton*

Evan Krieger  
*University of Dayton*

Paheding Sidike  
*University of Dayton*

Vijayan K. Asari  
*University of Dayton, vasari1@udayton.edu*

Follow this and additional works at: [https://ecommons.udayton.edu/ece\\_fac\\_pub](https://ecommons.udayton.edu/ece_fac_pub)

 Part of the [Electrical and Computer Engineering Commons](#), [Numerical Analysis and Computation Commons](#), and the [Theory and Algorithms Commons](#)

---

### eCommons Citation

Albalooshi, Fatema; Krieger, Evan; Sidike, Paheding; and Asari, Vijayan K., "Efficient Thermal Image Segmentation through Integration of Nonlinear Enhancement with Unsupervised Active Contour Model" (2015). *Electrical and Computer Engineering Faculty Publications*. 388.

[https://ecommons.udayton.edu/ece\\_fac\\_pub/388](https://ecommons.udayton.edu/ece_fac_pub/388)

This Conference Paper is brought to you for free and open access by the Department of Electrical and Computer Engineering at eCommons. It has been accepted for inclusion in Electrical and Computer Engineering Faculty Publications by an authorized administrator of eCommons. For more information, please contact [frice1@udayton.edu](mailto:frice1@udayton.edu), [mschlangen1@udayton.edu](mailto:mschlangen1@udayton.edu).

# Efficient Thermal Image Segmentation through Integration of Nonlinear Enhancement with Unsupervised Active Contour Model

Fatema A. Albalooshi, Evan Krieger, Paheding Sidike, Vijayan K. Asari

Dept. of Electrical and Computer Engineering, University of Dayton  
300 College Park, Dayton, OH, USA 45469-0232

## ABSTRACT

Thermal images are exploited in many areas of pattern recognition applications. Infrared thermal image segmentation can be used for object detection by extracting regions of abnormal temperatures. However, the lack of texture and color information, low signal-to-noise ratio, and blurring effect of thermal images make segmenting infrared heat patterns a challenging task. Furthermore, many segmentation methods that are used in visible imagery may not be suitable for segmenting thermal imagery mainly due to their dissimilar intensity distributions. Thus, a new method is proposed to improve the performance of image segmentation in thermal imagery. The proposed scheme efficiently utilizes nonlinear intensity enhancement technique and Unsupervised Active Contour Models (UACM). The nonlinear intensity enhancement improves visual quality by combining dynamic range compression and contrast enhancement, while the UACM incorporates active contour evolutionary function and neural networks. The algorithm is tested on segmenting different objects in thermal images and it is observed that the nonlinear enhancement has significantly improved the segmentation performance.

**Keywords:** Thermal image, nonlinear image enhancement, distinct object segmentation, level set function, self organizing map

## 1. INTRODUCTION

Image segmentation is a challenging task due to the reason that there is no generic solution that is suitable for all kinds of images and objects. The variations in objects can be large due to intensity differences and homogeneous or nonhomogeneous texture. Thermal infrared sensors provide valuable advantages over the visible camera because they are less sensitive to illumination variations and this enables them to play an important role for the characterization of regions of interests. This merit gives rise for effective segmentation of objects.

However, thermal imagery also introduces challenges, including low intensity contrast, low signal-to-noise ratio, blurring effects, over-centralized intensity distribution and halo effect.<sup>1-4</sup> Thus, directly applying segmentation methods on raw thermal imagery may cause inaccurate segmentation results. One of the efficient solutions is to introduce a preprocessing step to the segmentation process to alleviate detrimental effects in thermal imagery.

In this paper, we introduce a new technique to improve the performance of image segmentation in thermal imagery. The proposed scheme efficiently utilizes nonlinear intensity enhancement and Unsupervised Active Contour Models (UACM) to generate robust object region and boundary extraction in thermal imagery. The nonlinear intensity enhancement process consists of dynamic range compression, contrast enhancement, and color restoration processes. The dynamic range compression is achieved by a locally tuned inverse sine nonlinear function,<sup>5</sup> to provide various nonlinear curves based on neighborhood information. A neighborhood based pixel-dependent technique is employed to obtain sufficient contrast between objects and background in the thermal imagery, then a nonlinear color restoration process is used to restore color from the enhanced intensity image. During the enhancement, the halo effect is reduced by using the high frequency information of the original image

to reduce blurring at the edges between high and low intensity areas. The nonlinear intensity enhancement improves visual quality by combining dynamic range compression and contrast enhancement to remove the detrimental effects in thermal images, while the UACM incorporates active contour evolutionary function and Self-Organizing Map (SOM) to precisely segment regions of interest.<sup>6,7</sup> The nonlinear image enhancement technique allows enriched image features to be utilized by UACM to automatically direct evolutionary contour towards the region of interest, and thus improves segmentation process. The algorithm is tested on segmentation of different objects in real world thermal images and it is observed that the nonlinear enhancement is effective in improving the segmentation performance.

The rest of paper is organized as follows. Section 2 provides the details of the proposed nonlinear intensity enhancement and unsupervised active contour models for thermal image segmentation. In section 3, test results and statistics are presented and discussed. Finally, section 4 outlines concluding remarks of this technology.

## 2. METHOD

A functional framework of the proposed segmentation method is shown in Figure 1.

### 2.1 Nonlinear enhancement process

The process for the image enhancement method consists of dynamic range compression, contrast enhancement, and color restoration as show in Figure 2. The dynamic range compression includes intensity conversion, nonlinear enhancement, and high frequency boosting. The proposed nonlinear enhancement uses an arcsine function with a single tunable parameter. This parameter is determined based on the neighborhood information of the pixel being transformed. The design concept of this transformation function is based on previous research<sup>8,9</sup>

Figure 3 shows the effect of our enhancement. It can be seen that the visual quality of the image is improved after applying the nonlinear enhancement. The dynamic range compression improves the portions of the images with extreme high and low intensities. The image sharpening allows for the details of the object to be more apparent and the contrast enhancement improves the contrast between the object and the background.

#### 2.1.1 Dynamic range compression

The dynamic range compression process is performed to obtain new, enhanced intensity values using a nonlinear enhancement algorithm. Using a tuning parameter based on the Gaussian mean, the resulting image will see enhancement in both underexposed and overexposed regions of the image. Each step in the dynamic range compression is explained in the following three sections.

##### 2.1.1.1 Intensity conversion

The original color input image is converted to intensity (grayscale) image. The original RGB image,  $I(x, y)$ , is decomposed into luma (intensity),  $Y'(x, y)$ , and chrominance channels,  $U(x, y)$  and  $V(x, y)$ , using the  $YUV$  color space. This conversion is

$$\begin{bmatrix} Y'(x, y) \\ U(x, y) \\ V(x, y) \end{bmatrix} = \begin{bmatrix} 0.29890 & 0.58670 & 0.11400 \\ -0.14713 & -0.28889 & 0.43600 \\ 0.61500 & -0.51499 & -0.10001 \end{bmatrix} \begin{bmatrix} I_R(x, y) \\ I_G(x, y) \\ I_B(x, y) \end{bmatrix} \quad (1)$$

where  $I_R(x, y)$ ,  $I_G(x, y)$ , and  $I_B(x, y)$  represent the pixel value at location  $(x, y)$  of the  $R$ ,  $G$  and  $B$  channels of the color image.

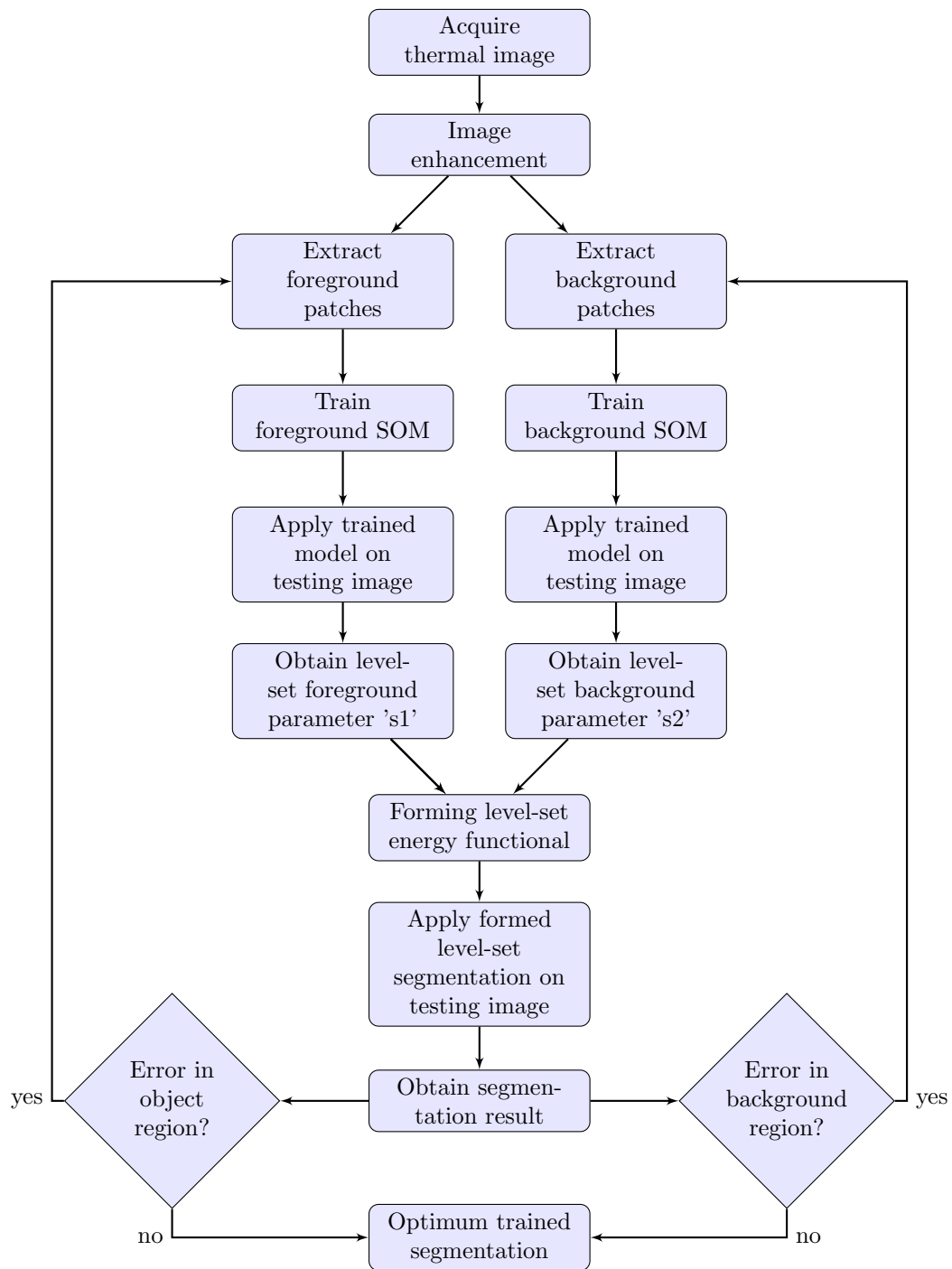


Figure 1. The functional framework of the proposed segmentation system.

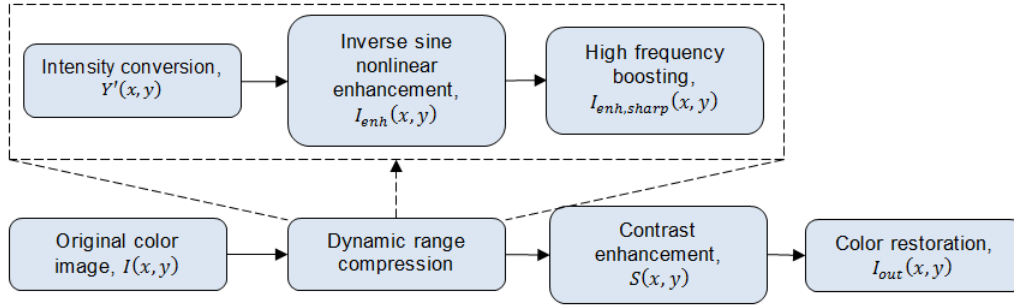


Figure 2. Structure of the proposed image enhancement algorithm.

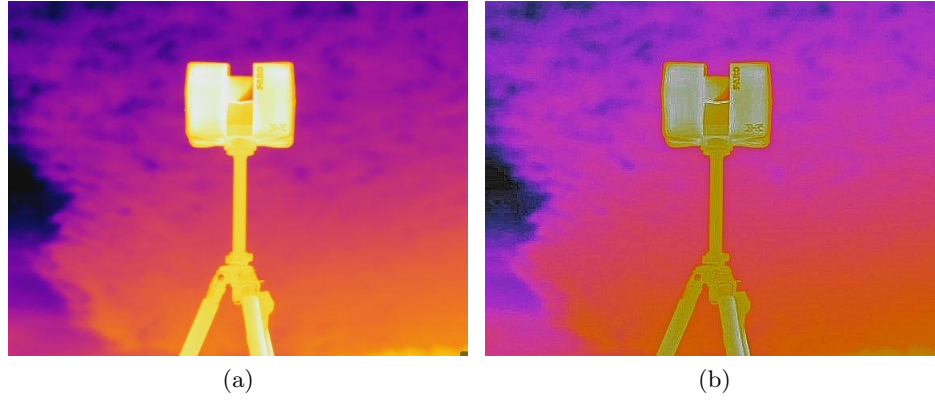


Figure 3. Effect of nonlinear enhancement (a) thermal image before enhancement (b) enhanced thermal image.

#### 2.1.1.2 Nonlinear enhancement

The intensity,  $Y'(x, y)$ , is used to create a normalized intensity image,  $I_n(x, y)$ , with the range  $[0, 1]$ . Next, the nonlinear transfer function is applied. The transfer function is

$$I_{enh}(x, y) = \frac{2}{\pi} \sin^{-1} \left( I_n(x, y)^{\frac{q}{2}} \right), \quad (2)$$

where  $I_n(x, y)$  is the normalized pixel value at location  $(x, y)$  and  $q$  is the locally adaptive control parameter. Figure 4 shows the nonlinear function at various values of  $q$ . As parameter  $q$  goes under 1 [Figure 4(a)], the nonlinear curves positively boost the input, increasing their intensity value. As parameter  $q$  goes over 1 [Figure 4(b)], the nonlinear curves negatively boost the input, decreasing their intensity value.

The control parameter  $q$  is based on tangent and natural logarithm functions using the input of the normalized mean intensity value. The mean intensity value is determined for each pixel by averaging the results of three Gaussian smoothed images. The three smoothed images are found using three different Gaussian kernels. These kernels are created with three different sizes based on the size of the original image. The Gaussian kernels used are square kernels with each side of size

$$k_1 = \frac{winsize_{max}}{200}, \quad (3)$$

$$k_1 = \frac{winsize_{max}}{75}, \quad (4)$$

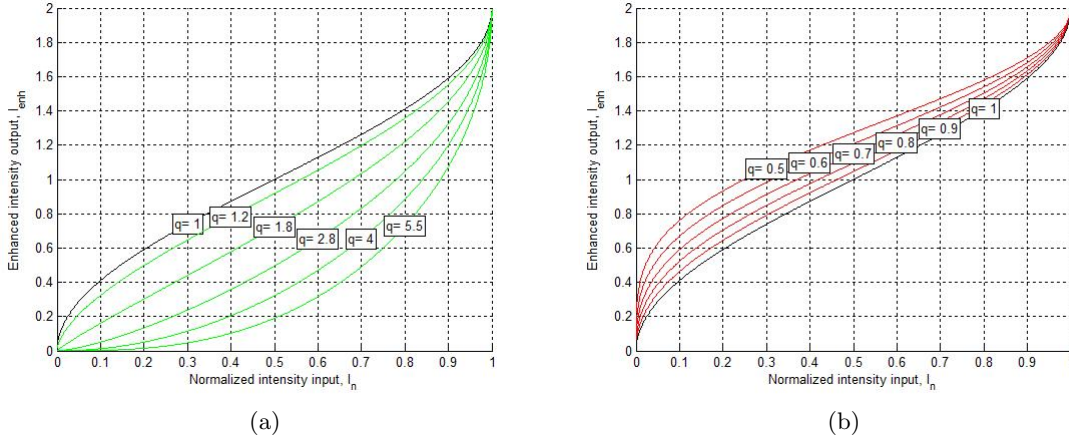


Figure 4. Various nonlinear curves at varying  $q$  values. (a)  $q$  less than 1 (b)  $q$  more than 1.

$$k_1 = \frac{winsize_{max}}{225}, \quad (5)$$

where  $winsize_{max}$  is the maximum window size (height or width). The kernels are created using

$$kernel_i(n_1, n_2) = \frac{h_g(n_1, n_2)}{\sum_{n_1} \sum_{n_2} h_g(n_1, n_2)}, \quad (6)$$

where  $h_g(n_1, n_2) = \exp\left(\frac{n_1^2 + n_2^2}{2\sigma_i^2}\right)$ ,  $n_1, n_2$  range from  $-k_i/2$  to  $k_i/2$ ,  $i$  indicates which kernel size is being used, and  $\sigma$  is found using

$$\sigma_i = 0.3(k_i/2 - 1) + 0.8. \quad (7)$$

The Gaussian mean intensity is then calculated using

$$I_{M,i}(x, y) = \sum_{m=-k_i/2}^{k_i/2} \sum_{n=-k_i/2}^{k_i/2} I(m+x, n+y) kernel_i(m, n). \quad (8)$$

The three intensity mean images are then averaged to obtain the intensity mean,  $I_M(x, y)$ . By using the mean intensity to select the  $q$  parameter, a halo effect occurs in the enhanced image in the high frequency areas of the image. This is due to the normalized multi-level Gaussian mean blurring the image at edges between high and low intensity areas. The halo effect is reduced by using the high frequency information of the original image to reduce this blurring at the edges. This is computed as

$$I_{hf}(x, y) = |I_{M,3}(x, y) - I_n(x, y)|. \quad (9)$$

The high frequency image is then normalized between to the range  $[0 \ 1]$  and is used to create the normalized intensity mean with high frequency adjustment as

$$I_{Mn}(x, y) = \frac{I_M(x, y) + cI_{hf}(x, y)I_n(x, y)}{1 + cI_{hf}(x, y)}, \quad (10)$$

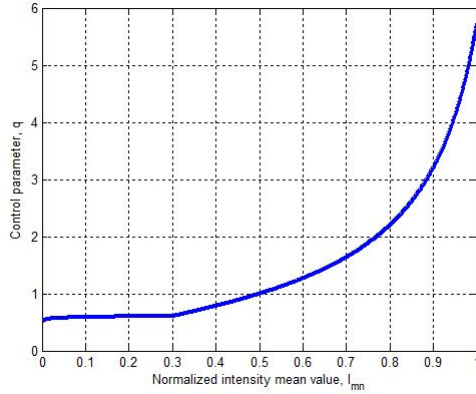


Figure 5. Control parameter 'q' as a function of normalized intensity mean.

where  $c$  is a constant that determines the amount of halo reduction that will be applied. It was found through empirical testing that a value of  $c = 9$  result in adequate halo removal for the enhancement of thermal images. The function for the control parameter  $q$  is then determined as

$$q = \begin{cases} \tan(\frac{\pi}{2.225} I_{Mn}(x, y)) + 0.162 & I_{Mn}(x, y) \geq 0.3 \\ \frac{1}{60.6} \ln(\frac{1}{0.3} I_{Mn}(x, y)) + 0.6061 & I_{Mn}(x, y) < 0.3 \end{cases} \quad (11)$$

The  $q$  function is shown in Figure 5. For pixels in extreme bright neighborhoods, the mean intensity value is near 1 and will be processed with a high  $q$  value. The results of a high  $q$  value in the nonlinear transfer function are curves that dampen the intensity value of the input. This is compressing the luminance as is desired. For extreme dark pixel regions, the mean intensity value is near zero and a low  $q$  value is obtained. This results in curves that will positively boost the input and enhance the luminance. It is also observed that for mean intensity values near 0.5, the  $q$  values result in curves that minimally change the input intensity values.

### 2.1.1.3 High frequency boosting

During the intensity enhancement process it is possible that sharply detailed regions that include rapid illumination changes can be degraded. To restore the details, a Laplacian high-boost filtering technique is used.<sup>10</sup> The convolution mask,

$$M = \begin{bmatrix} -1 & -1 & -1 \\ -1 & 8 & -1 \\ -1 & -1 & -1 \end{bmatrix} \quad (12)$$

is used to filter with the enhanced intensity image. The result is normalized with the range  $[0, 1]$  and is added to  $I_{enh}(x, y)$  to create the sharpened image,  $I_{enh,sharp}(x, y)$ .

### 2.1.2 Contrast enhancement

A neighborhood based pixel-dependent technique is used to obtain sufficient contrast in the enhance image. For this technique, the neighborhood intensity information is compared to the pixel value of the original intensity image. The result of the comparison is then used to contrast enhance the enhanced intensity image using the equations

$$S_i(x, y) = 255 I_{enh,sharp}(x, y)^{E_i(x, y)}, \quad (13)$$

$$E_i(x, y) = [\frac{I_{M,i}(x, y)}{Y'(x, y)}]^p, \quad (14)$$

where  $p$  is a tuning parameter. The three contrast enhanced images, obtained from using the three Gaussian kernels, are averaged to obtain the final contrast enhanced image,  $S(x, y)$ . The tuning parameter  $p$  can determine the severity of contrast enhancement and is based on the global standard deviation.

### 2.1.3 Color restoration

The color restoration process is required to get the intensity image back into a three channel color image. For thermal images, the color is restored by applying the original color map that was used for the original image. This allows for the enhanced image to have a similar appearance to the input color thermal image.

## 2.2 The self-organizing map

SOMs or Kohonen maps,<sup>11</sup> provide unsupervised spatial representations of feature vectors of input data in significantly lower dimensions output vectors known as Best Matching Units (BMUs). SOMs have been used in several applications such as speech recognition, pattern recognition, process control, robotics, processing semantic information, and many more.<sup>11</sup> The BMU is determined by calculating the minimum Euclidean distance between each node's weight vector and the current input vector:

$$Dist(u, w_i) = ||u - w_i|| \quad (15)$$

Thus,

$$BMU = \min_i \{Dist(u, w_i)\} \quad (16)$$

where  $u$  is the current input pattern and  $w_i$  is the node's weight vector.

Every node within the BMU's neighbourhood (including the BMU) has its weight vector adjusted according to the following equation:

$$w_i(t+1) = w_i(t) + \Theta(t)L(t)[u(t) - w_i(t)] \quad (17)$$

where  $t$  is the time step,  $L(t)$  is the learning rate, and  $\Theta(t)$  is the amount of influence a node's distance has from the BMU on its learning.

$L(t)$  is defined as:

$$L(t) = L_0 \cdot \exp(\frac{-t}{\lambda}); \quad t = 1, 2, 3, \dots \quad (18)$$

where  $t$  is the time step,  $L_0$  is the learning rate at time  $t_0$ .

$\Theta(t)$  is defined as:

$$\Theta(t) = \exp(\frac{-Dist^2}{2\sigma(t)^2}); \quad t = 1, 2, 3, \dots \quad (19)$$

where  $\sigma$  is the radius of the neighbourhood function.



## 2.3 Learning a level-set function by self organization

We suggest a modified level set prior-based segmentation approach that integrates neural networks with the level set active contour models for boundary extraction of objects in cluttered environment. One merit of our method is that small seed patches representing the object of interest and other small seed patches representing the background region from one single reference image is enough to complete the training process. The outcomes of the algorithm include the detection of the object of interest and correct extraction of its boundaries.

We aim at boundary and region extraction of objects in thermal imagery. The first step in our method includes clustering the intensity information of both the object of interest and its background through unsupervised *SOM* technique to produce two SOM maps; one SOM network to represent the object of interest, and another SOM network representing the background region. The trained networks are employed into the second stage of our segmentation process to map the intensity levels of an input thermal testing image. The mapped testing neurons are then utilized into the evolving curve energy functional of a level set protocol in the third stage of our proposed approach.

The most optimum boundary will be the boundary that holds the complete object region of interest even if it has various intensity and/or color variations. Thus, that boundary would be the most proper one for subsequent processes such as scene identification and interpretation. The segmentation process is facilitated by the construction of a cost functional; in which, the curve evolution is represented by the zero level of a level-set function that consumes local image information in order to get the optimum boundary and region representation of the object of interest. The problem of minimizing the cost functional is handled using Calculus of variations.<sup>12</sup> Our method is based on the locally image fitting level set energy functional.<sup>13</sup> By introducing the *SOM* image fitting energy to highlight the object of interest, our model is able to segment objects in images with intensity inhomogeneities. Moreover, a Gaussian filtering for variational level set is used to regularize the level set function, and to eliminate the requirement of re-initialization, which is very computationally expensive.

### 2.3.1 Applying modified level-set function

Our modified level set function is based on the locally image fitting energy functional.<sup>13</sup> We embed the clustered data coming from the *SOM* into the level set functional. We use the energy equation:

$$E^{SOM}(\phi) = \frac{1}{2} \int_{\Omega} |I(x, y) - I^{SOM}(x, y)|^2 dx dy, \quad x, y \in \Omega \quad (20)$$

where  $I^{SOM}$  is the our new self-organizing map fitted image and is defined as follows:

$$I^{SOM} = s_1 H_{\varepsilon}(\phi) + s_2 (1 - H_{\varepsilon}(\phi)) \quad (21)$$

$s_1$  and  $s_2$  are defined as follows:

$$s_1 = W_o - \text{mean}(I \in (\{(x, y) \in \Omega | \phi(x, y, t) < 0\} \cap G_k(x, y))) \quad (22)$$

$$s_2 = W_b - \text{mean}(I \in (\{(x, y) \in \Omega | \phi(x, y, t) > 0\} \cap G_k(x, y))) \quad (23)$$

where  $W_o$  and  $W_b$  are the best matching neurons of the foreground object region and background region respectively, and  $G_k(x, y)$  is a rectangular Gaussian window with width  $k$ .

Equation (20) is minimized with respect to  $\phi$  to get the corresponding gradient descent flow using the calculus of variation and the steepest method as shown below.<sup>13</sup>

The variation  $\eta$  is added to the level set function  $\phi$  such that  $\phi = \phi + \varepsilon\eta$ . Keeping  $m_1$  and  $m_2$  fixed, differentiating with respect to  $\phi$ , and letting  $\varepsilon \rightarrow 0$ , we have:

$$\begin{aligned} \frac{\delta E^{SOM}(\phi)}{\delta \phi} &= \lim_{\varepsilon \rightarrow 0} \frac{d}{d\varepsilon} \left( \frac{1}{2} \int_{\Omega} |I(x, y) - s_1 H_{\varepsilon}(\phi) - s_2 (1 - H_{\varepsilon}(\phi))|^2 dx dy \right) \\ &= \lim_{\varepsilon \rightarrow 0} \left( - \int_{\Omega} [I(x, y) - s_1 H_{\varepsilon}(\phi) - s_2 (1 - H_{\varepsilon}(\phi))] (s_1 - s_2) \delta_{\varepsilon}(\phi) \eta dx dy \right) \\ &= - \int_{\Omega} [I(x, y) - s_1 H_{\varepsilon}(\phi) - s_2 (1 - H_{\varepsilon}(\phi))] (s_1 - s_2) \delta_{\varepsilon}(\phi) \eta dx dy \end{aligned} \quad (24)$$

Therefore, the Euler-Lagrange Equation is obtained as follows:

$$-[I(x, y) - s_1 H_{\varepsilon}(\phi) - s_2 (1 - H_{\varepsilon}(\phi))] (s_1 - s_2) \delta_{\varepsilon}(\phi) = 0 \quad (25)$$

by the steepest gradient descent method, the following gradient descent flow is obtained:

$$\begin{aligned} \frac{\partial \phi}{\partial t} &= (I(x, y) - s_1 H_{\varepsilon}(\phi) - s_2 (1 - H_{\varepsilon}(\phi))) (s_1 - s_2) \delta_{\varepsilon}(\phi) \\ &= (I(x, y) - I^{SOM}(x, y)) (s_1 - s_2) \delta_{\varepsilon}(\phi) \end{aligned} \quad (26)$$

The main steps to apply level set segmentation are summarized as follows:

1. Let  $\Omega_0$  be a subset in the image domain  $\Omega$  and  $\partial\Omega_0$  be all the points on the boundary of  $\Omega_0$ . Then, the level set function  $\phi$  is defined be a binary function as follows:

$$\phi(x, y, t = 0) = \begin{cases} -\rho, & (x, y) \in \Omega_0 - \partial\Omega_0 \\ 0, & (x, y) \in \partial\Omega_0 \\ \rho, & (x, y) \in \Omega - \Omega_0 \end{cases} \quad (27)$$

where  $\rho > 0$  is a constant. The value of  $\rho$  is chosen to be larger than  $2\varepsilon$ , where  $\varepsilon$  is the width in the definition of the regularized Heaviside and Dirac delta functions defined in equations (28) and (30) respectively.

$$H_{\varepsilon}(\phi) = \frac{1}{2} \left( 1 + \frac{2}{\pi} \arctan\left(\frac{\phi}{\varepsilon}\right) \right) \quad (28)$$

$$\delta_{\varepsilon}(\phi) = \frac{d}{d\phi} H_{\varepsilon}(\phi), \quad (29)$$

$$= \frac{1}{\pi} \cdot \frac{\varepsilon}{\varepsilon^2 + \phi^2}, \quad \phi \in R \quad (30)$$

2. The level set function is evolved as stated in Equation(26).
3. Smooth the level set function using a Gaussian kernel, i.e.  $\phi = G_{\zeta} * \phi$ , where  $\zeta$  is the standard deviation. It is important to note that in order to enhance the smoothing capacity,  $\zeta$  should be larger than the square root of the time-step  $\Delta t$ .
4. Check whether the evolution is motionless, otherwise go to step 2.

### 3. EXPERIMENTAL RESULTS

To verify the effectiveness of the proposed technique, we use the FLIR T650sc thermal camera, which provides high sensitivity of temperature measurements, to capture real-life images and test our algorithm in varying textural regions.

Our proposed method starts with enhancing the thermal images using nonlinear enhancement process. Then, we train SOMs by selecting one or two patches in the image as a negative or positive sample, and train the system using those patches. After obtaining the trained parameters, the proposed SOM based level set function as explained in the last section is applied on the enhanced thermal image. The experimental results of the proposed algorithm are provided with using enhancement and without using enhancement.

Figure 6 shows comparative results for car segmentation. Figure 6(a) is a thermal input image. Figure 6(b) is the results of using SOM based ACM segmentation, and Figure 6(c) shows the segmentation mask of it. On the second row of Figure 6, Figure 6(d) shows an enhanced version of the input thermal image. Figure 6(e) shows segmentation result on the enhanced image and Figure 6(f) shows the segmentation mask. It is obvious that our proposed method produces more accurate segmentation results and precisely segments objects of interests.

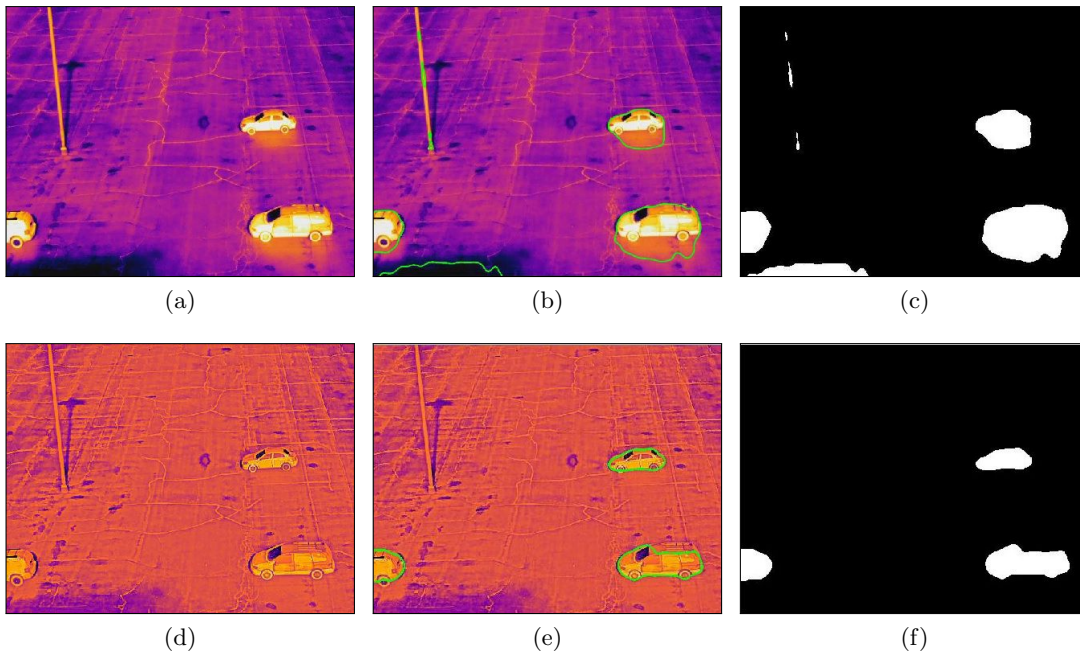


Figure 6. Results for car segmentation.

Figure 7 shows comparative results for people segmentation. Figure 7(a) is a thermal input image. Figure 7(b) is the results of using SOM based ACM segmentation, and Figure 7(c) shows the segmentation mask of it. On the second row of Figure 6, Figure 7(d) shows an enhanced version of the input thermal image. Figure 7(e) shows segmentation result on the enhanced image and Figure 7(f) shows the segmentation mask. Our proposed enhancement helps to produce precise segmentation of objects of interest compared to the non-enhanced thermal image which introduces false positives.

Table 1 shows average statistical values: specificity, precision, False Positive Rate (FPR), and False Negative Rate (FNR), applied on 66 thermal images. These statistical metrics show that our method yields better performance.

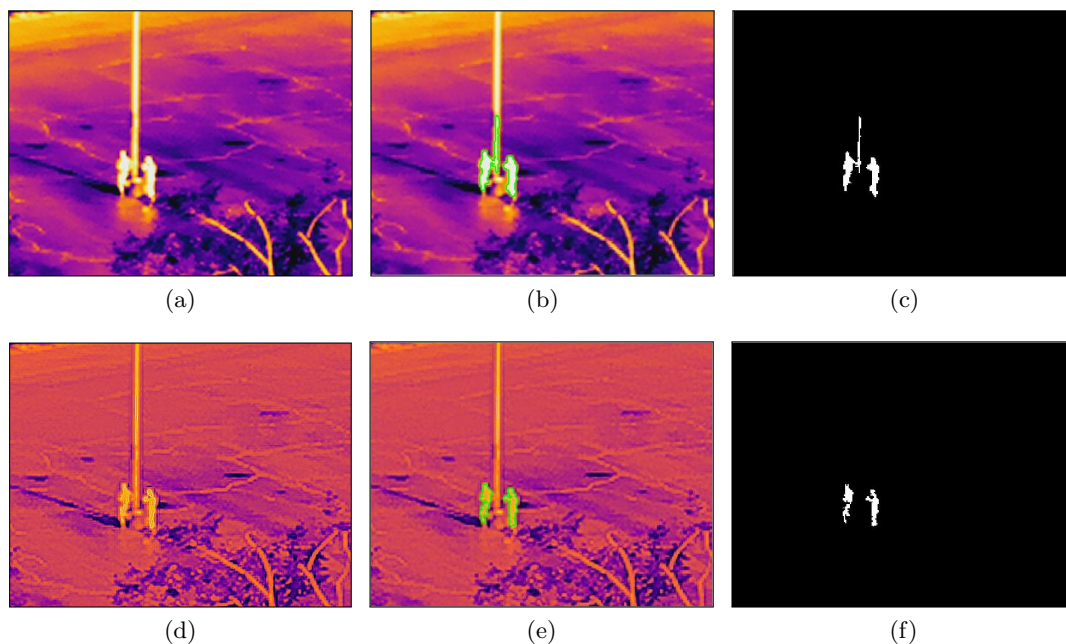


Figure 7. Results for people segmentation.

Table 1. Average segmentation statistical results for 66 thermal images.

|                     | Specificity | Precision | FPR   | FNR  |
|---------------------|-------------|-----------|-------|------|
| Non-enhanced images | 0.94        | 0.59      | 0.052 | 0.36 |
| Enhanced images     | 0.95        | 0.62      | 0.050 | 0.32 |

## 4. CONCLUSION

In this paper we presented a thermal image segmentation technique by utilizing nonlinear image enhancement and UACM. The proposed nonlinear intensity enhancement simultaneously dampened the overexposed regions, boosted the underexposed regions, and reduced halo effect. By combining dynamic range compression and contrast enhancement, we were able to remove the detrimental components in thermal imagery. The UACM utilized active contour evolution function and SOM to precisely segment regions of interest. Test results showed that the proposed algorithm is robust to handle segmentation challenges such as image blurring and halo effects of thermal imagery. It is also observed that directly applying the segmentation method on raw thermal imagery causes higher false positives and lower precision.

## REFERENCES

- [1] Cong-ping, C., Wu, Q., Zi-fan, F., and Yi, Z., "Infrared image transition region extraction and segmentation based on local definition cluster complexity," in [*Computer Application and System Modeling (ICCASM), 2010 International Conference on*], **3**, 50–54 (Oct 2010).
- [2] Li, Y. and Mao, X., [*An efficient method for target extraction of infrared images*], Springer (2010).
- [3] Fan, S. and Yang, S., "Infrared electric image segmentation using fuzzy renyi entropy and chaos differential evolution algorithm," in [*Future Computer Sciences and Application (ICFCSA), 2011 International Conference on*], 220–223 (June 2011).

- [4] Davis, J. W. and Sharma, V., "Background-subtraction in thermal imagery using contour saliency," *International Journal of Computer Vision* **71**(2), 161–181 (2007).
- [5] Arigela, S. and Asari, V. K., "A locally tuned nonlinear technique for color image enhancement," *WSEAS Trans. Sig. Proc.* **4**, 514–519 (Oct. 2008).
- [6] Albaloooshi, F., Sidike, P., and Asari, V., "Efficient hyperspectral image segmentation using geometric active contour formulation," in [*SPIE Remote Sensing Conference: Image and Signal Processing for Remote Sensing*], 924406–924413 (2014).
- [7] Albaloooshi, F., Smith, S., Diskin, Y., Sidike, P., and Asari, V., "Automatic segmentation of carcinoma in radiographs," in [*IEEE International Workshop on Applied Imagery and Pattern Recognition*], (Oct. 2014).
- [8] Arigela, S. and Asari, V. K., "Self-tunable transformation function for enhancement of high contrast color images," *Journal of Electronic Imaging* **22**(2), 023010–023010 (2013).
- [9] Krieger, E., Asari, V. K., and Arigela, S., "Color image enhancement of low-resolution images captured in extreme lighting conditions," *Proc. SPIE* **9120**, 91200–91215 (2014).
- [10] Marques, O., [*MATLAB Basics*], John Wiley and Sons, Inc. (2011).
- [11] Kohonen, T., "The self-organizing map," *Proceedings of the IEEE* **78**(9), 1464–1480 (1990).
- [12] Mumford, D. and Shah, J., "Optimal approximations by piecewise smooth functions and associated variational problems," *Communications on Pure and Applied Mathematics* **42**(5), 577–685 (1989).
- [13] Zhang, K., Song, H., and Zhang, L., "Active contours driven by local image fitting energy," *Pattern recognition* **43**(4), 1199–1206 (2010).